Nonlinear Vibrational Spectroscopic Studies of the Adsorption and Speciation of Nitric Acid at the Vapor/Acid Solution Interface

Melissa C. Kido Soule, Patrick G. Blower, and Geraldine L. Richmond*

Department of Chemistry, University of Oregon, 1253 University of Oregon, Eugene, Oregon 97403

Received: December 18, 2006; In Final Form: February 15, 2007

Nitric acid plays an important role in the heterogeneous chemistry of the atmosphere. Reactions involving HNO_3 at aqueous interfaces in the stratosphere and troposphere depend on the state of nitric acid at these surfaces. The vapor/liquid interface of HNO_3-H_2O binary solutions and $HNO_3-H_2SO_4-H_2O$ ternary solutions are examined here using vibrational sum frequency spectroscopy (VSFS). Spectra of the NO_2 group at different HNO_3 mole fractions and under different polarization combinations are used to develop a detailed picture of these atmospherically important systems. Consistent with surface tension and spectroscopic measurements from other laboratories, molecular nitric acid is identified at the surface of concentrated solutions. However, the data here reveal the adsorption of two different hydrogen-bonded species of undissociated HNO_3 in the interfacial region that differ in their degree of solvation of the nitro group. The adsorption of these undissociated nitric acid species is shown to be sensitive to the H_2O:HNO_3 ratio as well as to the concentration of sulfuric acid.

1. Introduction

Liquid/vapor interfaces, particularly those containing inorganic salts, acids, and organic species, have received special attention recently because of the many chemical and physical processes that occur at aqueous surfaces in the atmosphere. For example, reports suggesting that heterogeneous reactions involving halide ions at the sea-salt aerosol surface release halogens into the atmosphere have initiated an ongoing series of experimental and theoretical investigations into the affinity of ions for the air/water interface.[1−9] Similarly, much interest has been generated in the behavior of nitric and sulfuric acid at aqueous interfaces by the growing awareness of their key role in the surface chemistry of atmospheric aerosol particles.

Nitric acid is known as an end product of nitrogen oxide (NO_x) oxidation in the troposphere, and mechanisms for surface reactions such as the hydrolysis of nitrogen dioxide (NO_2) to nitrous acid (HONO) and HNO_3 have been well-studied.[10,11] Recently it has been shown that HNO_3 can also be reduced back to photochemcially active nitrogen in "renoxification" reactions at aqueous surfaces, with potential impact on the concentration of NO_x species and O_3 in the troposphere.[12−14] Laboratory experiments have demonstrated that these surface reactions depend sensitively on the form of HNO_3, whether dissociated or undissociated.[12] Nitric acid has also been shown to exist in both solid and liquid form in polar stratospheric clouds (PSCs). Solid PSCs are composed of H_2O and HNO_3 in crystalline form, and liquid PSC particles consist of supercooled ternary solutions of H_2SO_4, HNO_3, and H_2O.[15,16] Such stratospheric clouds comprise acidic surfaces on which chlorine and NO_x processing reactions linked to polar ozone destruction are known to occur.[15] From these examples it is clear that a molecular-level description of the structure and composition of binary HNO_3-H_2O and ternary $HNO_3-H_2SO_4-H_2O$ solution/vapor interfaces is essential to understanding the heterogeneous reactions that occur at such acidic aqueous surfaces throughout the atmosphere.

Any study of molecular properties at these surfaces requires a surface specific technique to distinguish between interfacial nitric acid species and bulk nitric acid. The surface sensitivity of traditional infrared techniques that can probe the liquid surface environment typically relies on the penetration depth of electromagnetic fields. For example, because of the mid-infrared wavelengths employed, the probe depth of attenuated total reflectance-FTIR spectroscopy (ATR-FTIR) is on the order of microns. In contrast, in second-order nonlinear techniques such as VSFS, the surface specificity is determined only by how deeply into the bulk medium molecules are influenced by the presence of the interface, i.e., the depth of orientational anisotropy. Defined by this criterion, the liquid interface is very thin, typically several angstroms.[17−19] With its inherent surface sensitivity, sum-frequency spectroscopy is uniquely capable of probing molecular structure in the top layers of a liquid interface.

In 1999, Shultz and co-workers used VSFS to examine water structure at the surface of HNO_3 aqueous solutions.[20] On the basis of spectral intensity changes in the OH stretching mode of interfacial water molecules, they postulated the existence of undissociated HNO_3 at the vapor interface of concentrated solutions. However, the expected OH signature of the molecular acid was not observed in the sum-frequency spectra. Concurrently, Donaldson and Anderson reported that the surface tension of sulfuric acid−water and pure water decreased upon addition of nitric acid and attributed this to the adsorption of molecular HNO_3 at those vapor/solution interfaces.[21] More recently, Finlayson-Pitts and co-workers identified an undisscociated nitric acid species at the concentrated solution surface using a combination of ATR-FTIR and SR-FTIR (single reflectance-FTIR) spectroscopies.[22] However, as discussed above, these techniques do not have the inherent sensitivity necessary to probe the top molecular layers of the vapor/liquid interface.

We report here the results of VSFS measurements of binary aqueous solutions of nitric acid (HNO_3-H_2O) and ternary

* Author to whom correspondence should be addressed. E-mail: richmond@uoregon.edu. Phone: 541-346-4635. Fax: 541-346-5859.

10.1021/jp0686994 CCC: $37.00
Published on Web 04/10/2007

mixtures of nitric acid, sulfuric acid, and water ($HNO_3-H_2SO_4-H_2O$). Vibrations of the nitro (NO_2) group of HNO_3 are used to examine the adsorption behavior and structure of undissociated nitric acid at the vapor/acid solution surface. The data provide direct evidence for two different hydrogen-bonded species of undissociated HNO_3 at the interface and suggest that these two species adsorb at different depths in the interfacial region.

2. Vibrational Sum-Frequency Spectroscopy: Background

Vibrational sum-frequency spectroscopy is described extensively in the literature and so only a brief summary is given here.[23−25] In VSFS, the vibrational spectrum of molecules at an interface between two isotropic media is obtained by spatially and temporally overlapping a tunable infrared beam (ω_{IR}) with a fixed-frequency visible beam (ω_{vis}) at the sample surface. These intense electric fields induce a nonlinear polarization in the medium that radiates at the sum of the infrared and visible frequencies, $\omega_{SF}= \omega_{IR} + \omega_{vis}$. The sum-frequency intensity is proportional to the intensities of the incident beams and to the square of the effective second-order susceptibility, $\chi^{(2)}_{eff}$:

$$I(\omega_{SF}) \propto |\chi^{(2)}_{eff}|^2 I(\omega_{vis})\, I(\omega_{IR}) \tag{1}$$

The effective susceptibility $\chi^{(2)}_{eff}$ is related to the true second-order susceptibility by Fresnel factors and unit polarization vectors for each beam. The second-order susceptibility $\chi^{(2)}$ can be expressed as the sum of a nonresonant component, $\chi^{(2)}_{NR}$, and a resonant component for each vibrational mode ν, $\chi^{(2)}_{R\nu}$.

$$\chi^{(2)} = \chi^{(2)}_{NR} + \sum_{\nu} \chi^{(2)}_{R\nu} \tag{2}$$

In general, both $\chi^{(2)}_{NR}$ and $\chi^{(2)}_{R\nu}$ are complex quantities and their relative phases must be taken into account. In these studies, we assume that ω_{vis} is far enough from any electronic transitions and therefore that the nonresonant component is real.

The resonant susceptibility, $\chi^{(2)}_{R}$, is related to the molecular hyperpolarizability, β, through the number density of probed molecules, N, and their orientation:

$$\chi^{(2)}_{R} = \frac{N}{\epsilon_o} \langle \beta \rangle \tag{3}$$

where the angular brackets denote an ensemble average over all possible molecular orientations. For conditions in which only the infrared frequency is near resonance to molecular transitions, the vibrational hyperpolarizability can be expressed as

$$\beta(\omega_{IR}) = \sum_{\nu} \frac{\langle g|\hat{\alpha}|\nu\rangle\langle\nu|\hat{\mu}|g\rangle}{\omega_{IR} - \omega_{\nu} + i\Gamma_{\nu}} \tag{4}$$

where the numerator represents the strength of the SF transition for vibrational mode ν, $|g\rangle$ and $|\nu\rangle$ are vibrational and ground states, and $\hat{\alpha}$ and $\hat{\mu}$ are the polarizability and dipole moment operators. Equation 4 illustrates that as the IR frequency is tuned and comes into resonance with vibrational modes of molecules at the surface, the sum-frequency response is enhanced, thus generating a vibrational spectrum of interfacial species.

Because the surface of a liquid has $C_{\infty v}$ symmetry, only 7 of the 27 elements of $\chi^{(2)}$ are nonzero and of these only 4 are unique. With the lab coordinates chosen so that z lies along the surface normal and the xz-plane is the plane of incidence, they are $\chi^{(2)}_{xxz} = \chi^{(2)}_{yyz}$, $\chi^{(2)}_{xzx} = \chi^{(2)}_{yzy}$, $\chi^{(2)}_{zxx} = \chi^{(2)}_{zyy}$, and $\chi^{(2)}_{zzz}$. In addition, for ω_{vis} far from resonance, $\chi^{(2)}_{xzx} = \chi^{(2)}_{yzy} = \chi^{(2)}_{zxx} = \chi^{(2)}_{zyy}$. These four elements can be probed using combinations of incident and outgoing linearly polarized light, namely: ssp, sps (or pss), and ppp, where the letters represent light polarized parallel to the plane of incidence (p) or perpendicular to the plane of incidence (s). All polarization schemes are given in the format sum-frequency, visible, infrared.

3. Experimental Section

3.1. Sample Preparation. Spectral grade HNO_3 (70 wt %) and H_2SO_4 (96 wt %) from Fisher Scientific were used as received. Binary HNO_3-H_2O and ternary $HNO_3-H_2SO_4-H_2O$ solutions were prepared daily with 18 MΩ water from a Nanopure system and stored away from light to avoid decomposition. Samples were placed in a custom-designed cell made of KEL-F with CaF_2 input and BK-7 output windows and sealed with VITON O-rings. Prior to their use, the sample cell and all glassware were cleaned with an H_2SO_4/NOCHROMIX solution followed by copious rinses with Nanopure water.

3.2. Spectroscopic Measurements. Details of the broad-bandwidth sum-frequency generation laser system have been described previously,[26] so only a brief overview will be given here. The ~100 fs output of a Ti:sapphire laser at 800 nm is amplified and split, with approximately 15% of the output used to produce ~2 ps pulses directed to the interface. The remaining output is used in an optical parametric amplifier (OPA) where tunable infrared light from 3 to 10 μm is produced. In the present studies, the OPA was tuned to the nitro (NO_2) antisymmetric stretching region ~1675 cm^{-1} where the IR energy was typically 6 μJ per pulse with ~175 cm^{-1} bandwidth. The IR beam and sample cell were entirely enclosed in a box with an overpressure of dry air, which reduced IR losses due to adsorption by water vapor in this wavelength region. The experiments were conducted in external reflection geometry and the generated sum-frequency light was collected with a spectrometer and a liquid nitrogen cooled CCD camera. The spectra here were obtained during 20 min CCD acquisitions. Spectra were normalized with the nonresonant VSFS spectrum from an amorphous gold surface, and calibrated using the positions of narrow features in the gold spectrum due to water vapor absorption. The error in calibrating the IR frequency is ±2 cm^{-1}. Prior to use in normalization, the Fresnel factors and unit polarization vector contributions were removed from the gold spectrum. Removal of these factors affected the spectral intensity but had no significant effect on the shape of the gold spectrum. At least three spectra per sample were taken on a given day and averaged, to document both reproducibility and sample stability. No significant evaporation of nitric acid from the solution surface (i.e., no loss of SF signal in successive spectra) was observed in repeated spectral acquisitions per sample. Furthermore, spectra presented here for all binary and ternary acid solutions were acquired over multiple days and averaged. All experiments were performed at room temperature.

As shown in eq 2, the second-order susceptibility is the sum of a nonresonant component and a resonant component; the resonant component is a sum of all of the contributing vibrational modes of the molecule. Because the SF intensity is related to the square of this coherent sum, interferences between nonresonant and resonant susceptibility elements can lead to distortions in peak shape and apparent peak frequency. Therefore, the VSFS spectra must be fit to accurately interpret the data. Following normalization and calibration, the VSFS spectra are analyzed using a line shape that accounts for the effects of

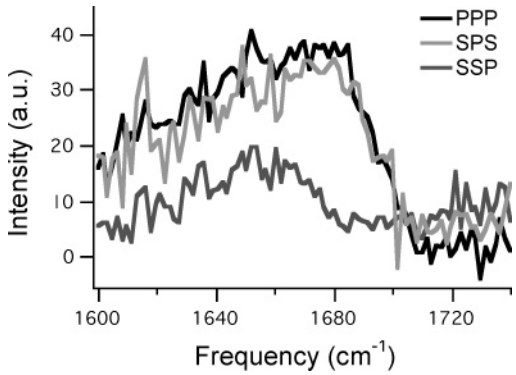

Figure 1. Sum-frequency spectra under ppp-, sps-, and ssp-polarizations of the vapor/solution interface of a 40 mol % HNO_3-H_2O binary mixture in the NO_2 antisymmetric stretching region.

homogeneous broadening (Lorentzian line shape) and inhomogeneous broadening (Gaussian line shape) because of the multitude of environments present in the condensed phase.[27−29] Following standard practice, symmetric peak shapes are used here as a first approximation to the lineshapes of species contributing to the VSFS spectrum.

$$|\chi^{(2)}(\omega_{SF})|^{(2)} = |\chi^{(2)}_{NR} + \int_{-\infty}^{\infty} \frac{A_\nu}{\omega_L - \omega_{IR} - i\Gamma_L} \exp\left[-\frac{(\omega_L - \omega_\nu)^2}{\Gamma_\nu^2}\right] d\omega_L|^2 \quad (5)$$

In eq 5, A_ν is the resonant amplitude, ω_ν is the resonant frequency, Γ_L (here, 2 cm^{-1}) and Γ_ν are the homogeneous and inhomogeneous line widths, and ω_L is a variable over which the integral is evaluated. Each of the resonant terms and the nonresonant term has a unique phase, ϕ, associated with it. Because both ω_{vis} and ω_{SF} are far from electronic resonance, the nonresonant term is constrained to be real with ϕ_{NR} of either 0 or π. All spectra are fit to the line shape in eq 5 with a nonlinear Levenberg−Marquardt least-squares algorithm implemented by Wavemetrics, Inc. in their program Igor. For all spectral analysis in this study, we use a global fitting procedure, which uses a series of tightly held constraints on the peak phases, widths, and locations obtained from spectra recorded in several different (yet related) environments. Fitting the spectra in this manner leaves only the peak amplitudes as truly free parameters and enables a rigorous and confident fit to the VSFS data.

4. Experimental Results

4.1. VSFS Spectra of Binary HNO_3 and H_2O Solutions. VSFS spectra of the 40 mol % nitric acid solution/vapor interface under ppp-, sps-, and ssp-polarization combinations are shown in Figure 1. A single feature is observed between 1600 and 1700 cm^{-1} in the three polarization spectra. Interestingly, although the ppp- and sps-polarization spectra appear to be qualitatively similar, the ssp spectrum looks quite different. The polarization series was globally fit using eq 5 to constrain the fitting parameters; resonant peak widths and locations were held constant across the three spectra, and peak amplitudes and phases were allowed to vary. Initial attempts to fit all three spectra with a single resonant component and a (real) nonresonant background failed to produce adequate results. This inadequacy was interpreted as possible evidence for the presence of another resonant contribution being present in the system. In Figure 2, two resonant $\chi^{(2)}$ components along with a nonresonant contribution are used to globally fit the polarization

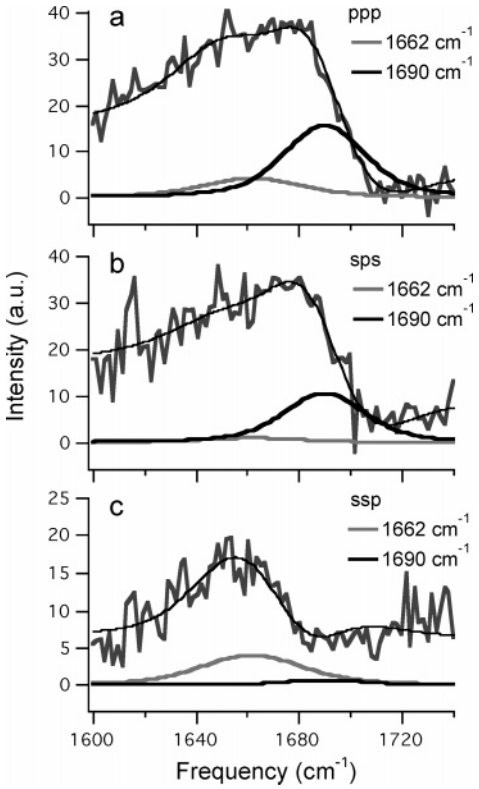

Figure 2. Global fitting results for sum-frequency spectra of a 40 mol % HNO_3-H_2O binary solution under (a) ppp-polarization, (b) sps-polarization, and (c) ssp-polarization. Resonant peaks in the NO_2 antisymmetric stretching region are shown below the spectra.

TABLE 1: Spectral Fitting Parameters for the VSFS Peaks in the NO_2 Antisymmetric Stretching Region of 40 mol % HNO_3 Solutions in ppp-, sps-, and ssp-Polarizations

	1690 ± 2 cm^{-1}	1662 ± 2 cm^{-1}
Γ_ν (cm^{-1})	18	23
A_ν ppp (au)	4.5	2.2
A_ν sps (au)	3.7	1.1
A_ν ssp (au)	0.85	2.2
ϕ_ν ppp (rad)	3.3	3.3
ϕ_ν sps (rad)	3.3	3.3
ϕ_ν ssp (rad)	6.28	4.28

series and produce excellent fits that are consistent across the set of data. The two resonant features are determined to be at 1690 ± 2 and 1662 ± 2 cm^{-1}. Parameters resulting from this fit of the polarization series, including the inhomogeneous width, Γ_ν, and the resonant amplitudes and phases, are presented in Table 1. The resonant phases shown are relative to a nonresonant phase of π.

In Figure 2, the polarization VSFS spectra have been deconvoluted to show each resonant contribution to the overall spectrum. In the ppp and sps spectra, the amplitude of the higher frequency feature dominates that of the lower frequency peak. The ~1690 cm^{-1} peak has about 2 times the amplitude as the ~1662 cm^{-1} peak in the ppp spectrum, and about 3 times the amplitude in the sps spectrum. However, this relationship between the two features is reversed in the ssp spectrum; the lower frequency peak at ~1662 cm^{-1} dominates the spectrum and is about 2.5 times greater than the ~1690 cm^{-1} peak.

Two assignments are possible for these features at ~1662 and ~1690 cm^{-1}. The antisymmetric NO_2 stretching mode of undissociated HNO_3 is observed the in 1650−1710 cm^{-1} region, depending on its environment.[30−32] Therefore, the spectral intensity in Figure 1 could arise from nitric acid adsorbed at

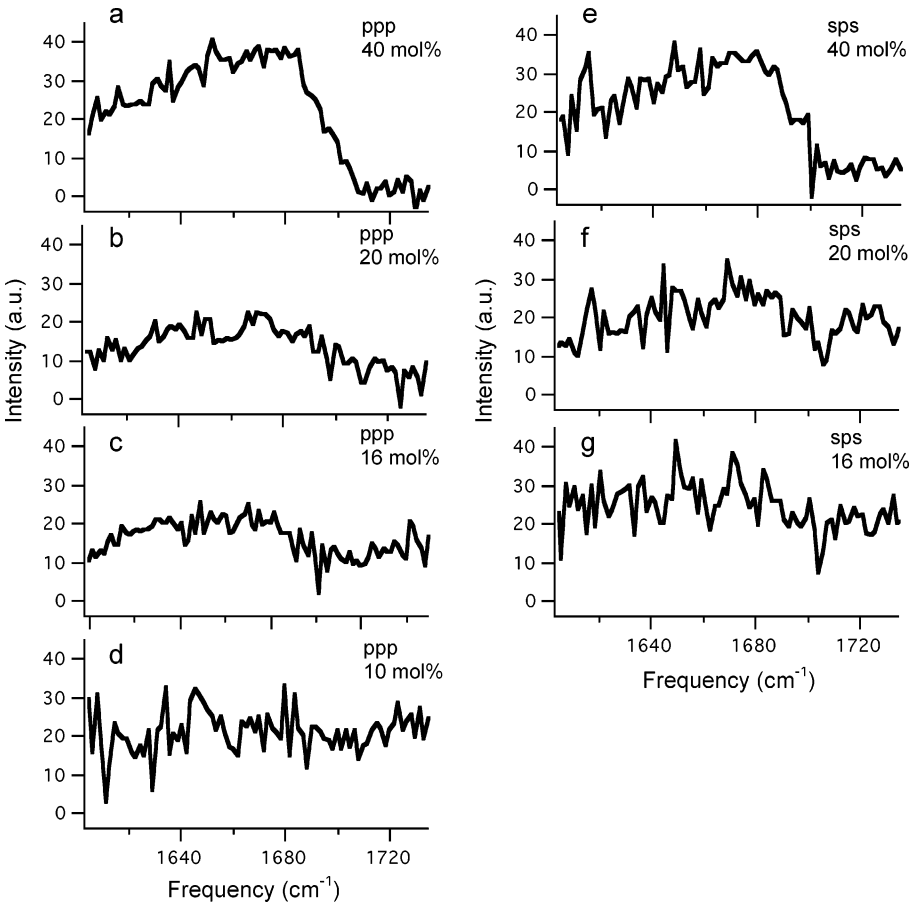

Figure 3. Sum-frequency spectra of the NO_2 antisymmetric stretching mode for HNO_3-H_2O binary solutions. For ppp-polarization, the acid concentrations are (a) 40 mol %, (b) 20 mol %, (c) 16 mol %, and (d) 10 mol %. For sps-polarization, the concentrations are (e) 40 mol %, (f) 20 mol %, and (g) 16 mol %.

the interface in molecular form. However, recent molecular dynamics simulations predict a slight surface affinity for NO_3^-,[33,34] and thus nitrate ions from HNO_3 dissociation could also contribute to the VSFS spectra. The planar, symmetric nitrate ion has four vibrational frequencies near 1370 (ν_3), 1043 (ν_1), 830 (ν_2), and 723 (ν_4) cm^{-1}.[35] Although none of the fundamental frequencies are near the 1600−1700 cm^{-1} region, the overtone of the ν_2 band at 1657 cm^{-1} ($2\nu_2$) has been observed in the resonance Raman spectrum of KNO_3 in water.[35] In aqueous solution, a reduction in nitrate ion symmetry to C_{2v} renders ν_2 (and $2\nu_2$) both IR and Raman active, and therefore sum-frequency active.[35]

To resolve these possible spectral assignments, VSFS experiments as a function of HNO_3 concentration were conducted. The dissociation of nitric acid observed in ATR-FTIR measurements[22] and in bulk aqueous solutions show that a decrease in nitric acid concentration leads to a corresponding decrease in the number of undissociated HNO_3 molecules and an increase in the NO_3^- ion concentration. At high concentration, 40 mol %, nitric acid is ∼17% dissociated, resulting in ∼13 M HNO_3 and ∼2.6 M NO_3^- in the bulk liquid.[31] At 20 and 16 mol %, the percent dissociation increases to ∼54% and ∼62%, respectively, and at a bulk concentration of 10 mol %, nitric acid is largely dissociated (∼75%).[36] Between 16−20 mol % HNO_3, the NO_3^- concentration increases to ∼5 M and the molecular HNO_3 concentration decreases to ∼4 M. By 10 mol %, the concentration of nitrate ion is three times that of the molecular acid. If nitrate ions contribute to the 40 mol % VSFS spectra in Figure 1 through the ν_2 overtone, then one would expect the increase in NO_3^- concentration with acid dissociation to be reflected in the interfacial spectra as a function of water content.

Figure 3 illustrates the effects of increasing water concentration on the surface adsorption of nitric acid. The nitric acid concentrations are shown in decreasing order from 40 to 10 mol % for ppp-polarization (Figure 3a−d), and from 40 to 16 mol % for sps-polarization (Figure 3e−g). The VSFS spectra show that the overall intensity in both polarizations decreases as water is added. Global fitting results for the ppp-polarization concentration series are shown in Figure 4, in which the peak phases and positions were held constant throughout the series and constrained using the results in Table 1 from the 40 mol % HNO_3 polarization series analysis. Peak widths were held constant to within 2.5% across the series and only the peak amplitudes were allowed to vary. In this way, high quality fits to the data in Figure 4 were obtained. The parameters resulting from this analysis of the ppp concentration series are consistent with those from the polarization series fit in Figure 2, with two resonant features in the NO_2 antisymmetric stretching region at 1690 ± 2 and 1662 ± 2 cm^{-1}, thus providing further confidence to these peak positions.

The results in Figure 4 show that the amplitudes of both features decrease as the nitric acid concentration decreases, contrary to what would be expected if the ∼1662 cm^{-1} peak were due to contributions from NO_3^- ions. However, the spectral trends are consistent with an assignment of the two resonant features to the antisymmetric NO_2 stretching vibration of undissociated nitric acid. Therefore, we attribute the spectral features in Figures 1−4 to undissociated HNO_3 adsorbed in the

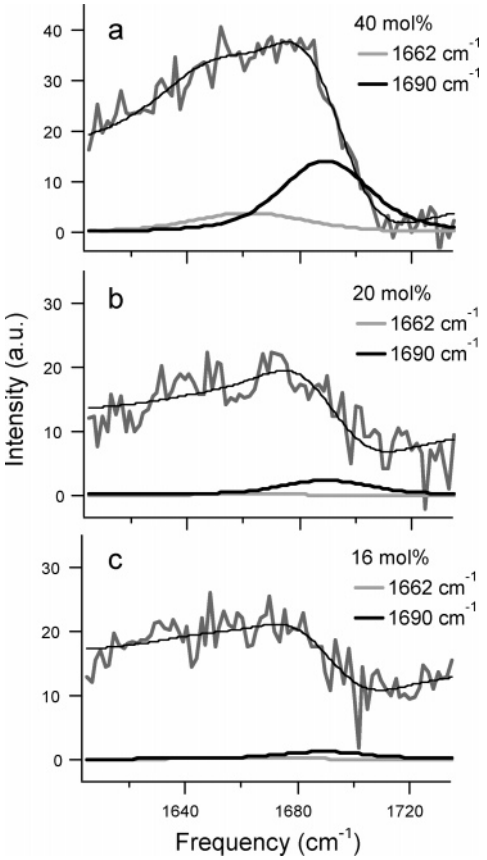

Figure 4. Global fitting of ppp-polarization sum-frequency spectra of HNO_3-H_2O binary solutions at (a) 40 mol %, (b) 20 mol %, and (c) 16 mol %.

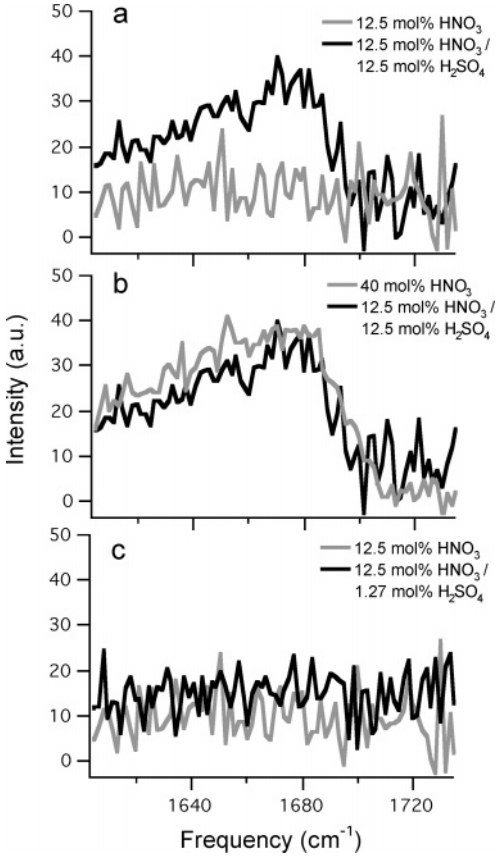

Figure 5. Sum-frequency spectra of the NO_2 antisymmetric stretch in ppp-polarization of $HNO_3-H_2SO_4-H_2O$ ternary solutions at constant HNO_3 concentration compared with HNO_3 binary solutions: (a) 12.5 mol % HNO_3/12.5 mol % H_2SO_4 compared with 12.5 mol % HNO_3; (b) 12.5 mol % HNO_3/12.5 mol % H_2SO_4 compared with 40 mol % HNO_3; (c) 12.5 mol % HNO_3/1.27 mol % H_2SO_4 compared with 12.5 mol % HNO_3.

top surface layers of HNO_3-H_2O binary solutions. Furthermore, global analyses of the polarization (Figure 2) and concentration (Figure 4) series indicate that two different hydrogen-bonding species of molecular HNO_3 are adsorbed at the binary solution surface. The nature of these species will be discussed further in the Discussion.

As shown in Figure 2, the polarization series analysis reveals an opposite relationship between the amplitudes of the ~1690 and ~1662 cm^{-1} features under ssp- and sps-polarizations. In light of the spectral assignments above, this trend qualitatively suggests different NO_2 group orientations for the two molecular nitric acid species at the air/solution surface. The data also show that the surface adsorption of these HNO_3 species is affected by the amount of water present. Figure 4 shows that molecular HNO_3 persists at the surface of solutions with as much as ~60% acid dissociation in the bulk, with the 1690 cm^{-1} peak at higher frequency dominating the peak at lower frequency throughout the concentration series. As illustrated in eqs 3 and 4, the sum-frequency intensity depends on the number of interfacial molecules, their orientation, and the Raman and IR transition strengths for a given vibrational mode. Because the VSFS intensity decreases for both sps- and ppp-polarizations as the nitric acid concentration is reduced below 40 mol %, this indicates that the decrease in intensity with increasing dilution is not due to a significant change in nitric acid orientation at the surface, but either to a decrease in the number of undissociated HNO_3 molecules in the interfacial region or to a change in the Raman and/or IR transition strengths. The bulk dissociation behavior of HNO_3 supports the conclusion that the decrease in VSFS intensity with nitric acid concentration observed in Figure 3 results from a corresponding decrease in the number of undissociated HNO_3 molecules at the vapor/liquid surface.

4.2. VSFS Spectra of Ternary HNO_3, H_2SO_4, and H_2O Solutions. Figures 5 and 6 show sum-frequency spectra in the NO_2 antisymmetric stretching region of ternary solutions of nitric acid, sulfuric acid, and water. In what follows, only the concentrations of the two acids are specified; the mole fraction of water in these solutions can be determined by subtracting the sum of the acid mole fractions from unity.

In Figure 5, the HNO_3 concentration is held constant at ~12.5 mol % in two solutions with either 12.5 or 1.27 mol % H_2SO_4. A ppp-polarization spectrum of the 12.5% HNO_3–12.5% H_2SO_4 ternary solution is shown in Figure 5a. Significant enhancement in signal from undissociated nitric acid is observed in comparison to the spectrum of a binary solution with 12.5 mol % HNO_3, which shows no NO_2 antisymmetric stretching intensity from undissociated nitric acid. The degree of this signal enhancement from undissociated HNO_3 at the ternary solution surface is considerable, especially when compared in Figure 5b to the ppp-spectrum of a 40 mol % HNO_3 binary solution, in which the HNO_3 bulk concentration is much greater. The increase in molecular nitric acid signal at the ternary solution surface in Figure 5a demonstrates that nitric and sulfuric acids are interacting in the interfacial region and that H_2SO_4 perturbs the molecular HNO_3 at the surface. However, as shown in Figure 5c, for a ternary mixture with a composition of 12.7 mol % HNO_3 and only 1.27 mol % H_2SO_4, a factor of 10 decrease in the H_2SO_4 concentration does not result in any change in the signal intensity from undissociated nitric acid at the surface.

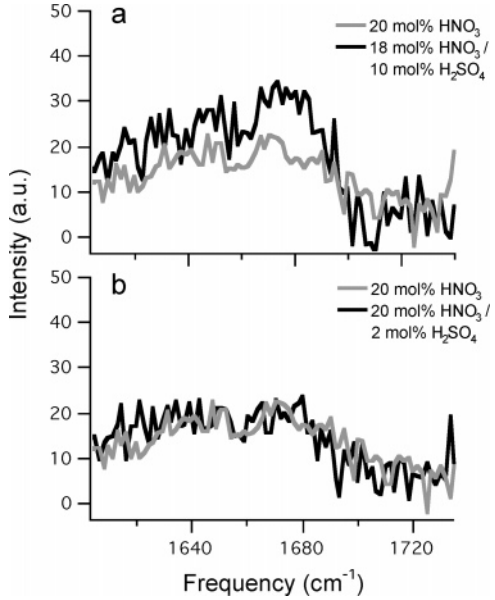

Figure 6. Sum-frequency spectra of the NO_2 antisymmetric stretch in ppp-polarization of $HNO_3-H_2SO_4-H_2O$ ternary solutions at constant 4:1 H_2O:HNO_3 ratio compared with a 20 mol % HNO_3 binary solution: (a) 18 mol % HNO_3/10 mol % H_2SO_4; (b) 20 mol % HNO_3/2 mol % H_2SO_4.

Because the VSFS intensity depends on the number of molecules and their orientation, as well as on the Raman and IR transition strengths, the intensity changes in Figure 5 could be a convolution of these effects. However, Raman studies of $HNO_3-H_2SO_4-H_2O$ mixtures that demonstrate the effects of H_2SO_4 on nitric acid in the bulk can be used to narrow the possibilities.[37] Raman spectra of comparable binary and ternary solutions show that although molecular nitric acid bands are barely discernible in a 1:10 HNO_3:H_2O binary solution, they are clearly observed in a ternary mixture with a 1:1:10 HNO_3:H_2SO_4:H_2O molar ratio. These Raman studies indicate that sulfuric acid perturbs the bulk HNO_3/NO_3^- equilibrium; they show that as the sulfuric acid concentration decreases, the molecular HNO_3 features in the ternary spectrum decrease while the NO_3^- ion bands increase. This shift in the HNO_3 dissociation equilibrium with H_2SO_4 suggests that at the ternary solution surface, the increase in VSFS intensity of the molecular nitric acid signal is due to an enhancement in the adsorption of the undissociated acid rather than to a significant change in molecular orientation or in the Raman cross-section resulting from $HNO_3-H_2SO_4$ interactions in the interfacial region.

An alternative explanation for the VSFS intensity changes in Figure 5 is a difference in the ratio between water and nitric acid, which could affect the degree of acid dissociation. Although the HNO_3-H_2O solution and $HNO_3-H_2SO_4-H_2O$ solutions in Figure 5 are held at constant nitric acid concentration (~12.5 mol %), the mole ratio of H_2O to HNO_3 is not the same. For example, the H_2O:HNO_3 ratio in the 12.5 mol % binary solution is 7:1, whereas in the 12.7 mol % HNO_3/1.27 mol % H_2SO_4 ternary solution the ratio decreases to 6.75:1, and further decreases to 6:1 in the 12.5 mol % HNO_3/12.5 mol % H_2SO_4 solution. To test this possibility, spectra of binary and ternary solutions with a constant 4:1 H_2O:HNO_3 ratio are compared in Figure 6. As seen in Figure 6a, in comparison to the binary solution with 20 mol % HNO_3, the VSFS signal from undissociated HNO_3 is indeed enhanced at the surface of a ternary solution containing 18 mol % HNO_3 and 10 mol % H_2SO_4. However, for a ternary solution with 20 mol % HNO_3 and only 2 mol % H_2SO_4, shown in Figure 6b, there is no significant change in VSFS signal. For reasons presented earlier in the discussion of Figure 5, the spectral intensity effects in Figure 6 are also attributed to changes in the adsorption of undissociated nitric acid in the interfacial region. Thus, both Figures 5a and 6a indicate that an enhancement in molecular HNO_3 at the ternary solution surface results from the addition of ≥10 mol % H_2SO_4. However, this enhancement is clearly dependent on the amount of H_2SO_4 present. As shown in Figures 5c and 6b, at low concentrations ~1−2 mol % H_2SO_4, there is much less impact of sulfuric acid on molecular nitric acid adsorption at the surface.

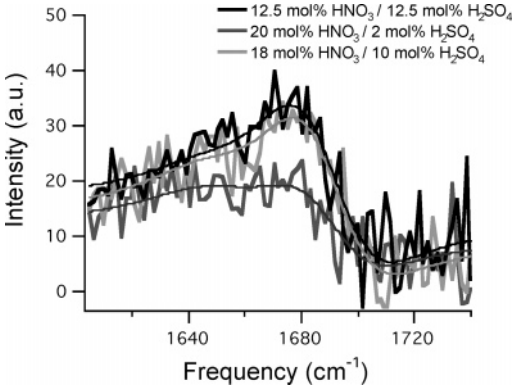

Figure 7. Global fits for ppp-polarization sum-frequency spectra of $HNO_3-H_2SO_4$ ternary solutions: 12.5 mol % HNO_3/12.5 mol % H_2SO_4, 18 mol % HNO_3/10 mol % H_2SO_4, and 20 mol % HNO_3/2 mol % H_2SO_4.

The VSFS spectra of the ternary solutions at constant mol % (Figure 5a) and at constant H_2O:HNO_3 ratio (Figure 6) were globally fit, as shown in Figure 7. The spectrum of the 20 mol % HNO_3 binary solution was globally fit along with the spectra in Figure 7 as a check for consistency with the binary solution analyses in Figures 2 and 4 (not shown for clarity). Again, consistent with the binary solution results, two different species of molecular nitric acid at the ternary solution surface are identified with peak positions at 1690 ± 2 and 1662 ± 2 cm^{-1}. The fitting shows that the amplitudes of both NO_2 antisymmetric stretching features increase with the addition of H_2SO_4 in the ternary solutions of Figures 5 and 6, relative to the binary HNO_3 solutions, and that the percent increase in amplitude of both features is greater in the mixtures with a higher concentration of H_2SO_4 (10 or 12.5 mol %). Although the 1690 cm^{-1} feature dominates in the ternary mixtures with either 2 or 10 mol % H_2SO_4 in Figure 6, the fitting also shows that relative to the binary 20 mol % HNO_3 solution, the percent increase in amplitude is greater for the peak at 1662 cm^{-1} than for the peak at 1690 cm^{-1}.

5. Discussion

5.1. Binary Nitric Acid Mixtures. In bulk aqueous solutions, nitric acid is known to form complexes with water of the general form $HNO_3\cdot(H_2O)_n$, where $n = 1$ is the monohydrate, $n = 2$ is the dihydrate, and $n = 3$ is the trihydrate. The relative abundance of these complexes varies with the concentration of the solution. For example, at 40 mol % the most abundant component of the molecular nitric acid population is the monohydrate (~80%), with 8% of the trihydrate species and 12% of the unhydrated monomer.[38] By comparison, at 16 mol %, the mono- and trihydrate species are more comparable in abundance.

Evidence for the monohydrate complex between HNO_3 and H_2O has been reported in microwave studies of gas-phase HNO_3-H_2O clusters,[39] infrared studies of solid HNO_3-H_2O

mixtures,[40,41] and infrared studies of low-temperature argon matrices.[30] The infrared studies of ice films with a 1:1 ratio of water to nitric acid assign a feature ~1670−1673 cm^{-1} to the NO_2 antisymmetric stretch of the monohydrate complex. It is not surprising that this monohydrate frequency is very similar to that found for concentrated bulk aqueous solutions of HNO_3, given that at 40 mol % the monohydrate is the major form of undissociated nitric acid. Microwave experiments[39] and ab initio calculations[42] suggest a quasi-planar ring structure for this monohydrate complex, in which H_2O forms two hydrogen bonds to HNO_3. The primary hydrogen bond occurs between the H atom of nitric acid and the O atom of water with a bond length ~1.7 Å. Theoretical calculations suggest that, although not a "good" hydrogen bond because it is long (~2.4 Å) and bent, a second, much weaker interaction between the O atom of the nitro group and an H atom of water may provide additional stability to the complex.[42]

Interestingly, in the argon-matrix isolation studies the monohydrate is assigned to a feature at 1694 cm^{-1}, much higher than the ~1673 cm^{-1} feature reported in the infrared studies of solid HNO_3−H_2O mixtures. One explanation is the difference in the monohydrate structure suggested by the argon-matrix experiments, which consists of only a single hydrogen bond between the O atom of water and the H atom of HNO_3; no evidence is found in the matrix spectra for a second weak interaction between water and the NO_2 group of nitric acid.[30] Recent ab initio calculations suggest a nonplanar structure for this singly hydrogen-bonded monohydrate complex, where the hydrogen atoms of water are found out of the plane defined by the HNO_3 molecule.[43] The shift in NO_2 antisymmetric stretching frequency for HNO_3 in the gas phase (1710 cm^{-1}), liquid phase (1675 cm^{-1}), and solid phase (1646 cm^{-1}) illustrates that as the association strength of the nitro group increases, the fundamental frequency decreases.[31,32] Thus, a lack (or significant weakening) of interaction to the nitro group in a monohydrate complex would reasonably blue shift the NO_2 antisymmetric stretching frequency compared with a monohydrate in which NO_2 group is hydrogen bonded.

Using these experimental and theoretical investigations of HNO_3·H_2O complexes, assignments of the two resonant features in the sum-frequency spectra of HNO_3 solutions are made. We assign the spectral feature at 1690 ± 2 cm^{-1} to a monohydrate complex with a single hydrogen bond between water and the acid OH group. The absence of hydrogen bonding between H_2O and the acid NO_2 group indicates that this portion of the undissociated HNO_3 species can protrude out into the vapor phase, thereby placing the 1690 cm^{-1} complex in the topmost surface layer. The second feature in the VSFS spectrum at 1662 ± 2 cm^{-1} is assigned to a more strongly hydrogen-bonded complex between molecular nitric acid and water. This frequency is between that reported in infrared studies of ice for the monohydrate at 1673 cm^{-1} and the trihydrate at 1652 cm^{-1}.[40,41] Although unambiguous determination of the number of water molecules involved in this surface complex is not possible, the low frequency of the 1662 cm^{-1} complex suggests hydrogen bonding between both the acid OH and NO_2 groups and at least one water molecule. Given the additional hydrogen bonding interaction to the NO_2 group, this molecular nitric acid species may reside deeper into the interfacial region than the more weakly solvated complex at 1690 cm^{-1}. Figure 8 depicts these two HNO_3·H_2O complexes of undissociated nitric acid observed at the vapor/acid solution interface.

Additional support for this picture is provided by a recent ATR-FTIR spectroscopy study in which signatures of undissociated HNO_3 at the surface of concentrated nitric acid solutions were assigned to a monohydrate complex between molecular HNO_3 and H_2O.[22] The NO_2 antisymmetric stretching vibration was found at ~1673 cm^{-1}, very close to that for bulk solutions of HNO_3. However, no additional absorption near 1690 cm^{-1} indicative of a weakly bonded surface species was reported in their ATR-FTIR surface spectra. One possible explanation for this difference is that the interface as defined by the ATR-FTIR experiments is inherently deeper than for the sum-frequency experiments. The VSFS studies here provide evidence for the existence of two hydrogen-bonded species of molecular nitric acid at the solution surface. Moreover, these studies are the first to reveal a weakly solvated HNO_3 monohydrate complex that is unique to the sum-frequency spectrum and to the top layer of the vapor/liquid interface of the acid solution. Further studies to investigate these solvated surface HNO_3 species are planned with isotopic mixtures. Surface studies of crystalline ice clusters of H_2O and D_2O mixtures show a clear preference for surface HOD molecules to engage in deuterium bonding (over hydrogen bonding) with subsurface molecules.[44,45] Replacing H_2O with D_2O in the HNO_3 binary (and HNO_3/H_2SO_4 ternary) solutions here should produce shifts in the NO_2 antisymmetric stretching frequency consistent with the nitro group hydration environment at the vapor/acid solution interface.

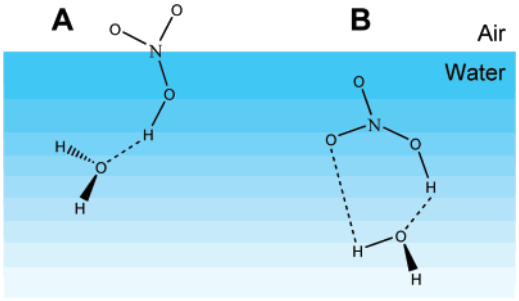

Figure 8. Picture of HNO_3·H_2O complexes at the vapor/HNO_3 solution interface observed in the VSFS spectra: a single hydrogen bond between the oxygen of water and the hydrogen atom of HNO_3 (A), and two hydrogen bonds between water and the OH and NO_2 groups of HNO_3 (B).

5.2. Ternary Nitric Acid/Sulfuric Acid Mixtures. The VSFS spectra show that the perturbation of molecular HNO_3 adsorption at the ternary solution surface by H_2SO_4 depends on the sulfuric acid concentration. This observation is consistent with reported surface tension measurements of ternary solutions.[21,46] For example, the surface tension of a ternary solution with 30 wt % HNO_3 and 40 wt % H_2SO_4, comparable to the solution in Figure 4a containing 12.5 mol % (~32 wt %) HNO_3 and 12.5 mol % (~43 wt %) H_2SO_4, is 61.82 dyn cm^{-1}.[46] This value is similar to the surface tension of a 40 mol % (70 wt %) HNO_3 binary solution with a much higher concentration of nitric acid.[21] By contrast, the surface tension of a ternary solution with 30 wt % HNO_3 and only 5 wt % H_2SO_4 (comparable to the 12.7 mol % (~32 wt %) HNO_3 and 1.27 mol % (~6 wt %) H_2SO_4 solution in Figure 4b) is 68.15 dyn cm^{-1}.[46] The surface tension of the ternary mixture with lower H_2SO_4 content is not significantly different from that of a binary mixture with ~12.5 mol % HNO_3.[21]

Because sulfuric acid clearly affects the adsorption of undissociated nitric acid at the ternary solution surface, an important question is the form of H_2SO_4 in these mixtures. Raman and FTIR specular reflectance studies of bulk ternary solutions indicate that the dissociation equilibria of HNO_3 and

H_2SO_4 interfere with each other.[37,47] The degree of dissociation of HSO_4^- is altered by the presence of HNO_3 such that the ionization of HNO_3 occurs before the ionization of HSO_4^-, regardless of the acid concentration ratios; SO_4^{2-} dominates NO_3^- in the competition for protons in solution.[37] This indicates that for the ternary solutions here, sulfuric acid is predominantly in the form of bisulfate as opposed to sulfate.

Recent molecular dynamics simulations suggest that HSO_4^-, unlike SO_4^{2-}, is not strongly repelled from the air/solution interface but shows a similar moderate propensity for the surface as does the chloride ion.[48] The effect of sulfuric acid on interfacial water structure has also been examined by VSFS.[49,50] With increasing bulk concentration of sulfuric acid, the signal from water molecules in the top surface layer diminished, implying increased perturbation of the surface water structure.[49] The results were interpreted on the basis of ion pairing and the formation of acid hydrates at increasing H_2SO_4 concentration. For the ternary solutions with $\geq$10 mol % H_2SO_4 examined here (Figures 4a and 5a), associations between water and HSO_4^- in the interfacial region or molecular hydrate formation ($H_2SO_4 \cdot (H_2O)_n$) would serve to bind water molecules otherwise available at the corresponding HNO_3 binary solution surface. The resulting decrease in the effective H_2O:HNO_3 ratio would inhibit the dissociation of HNO_3 at the surface, and explains the observed enhancement of molecular nitric acid at the ternary solution surfaces with $H_2SO_4 \geq$ 10 mol %. This effect of H_2SO_4 on the HNO_3 dissociation equilibrium also explains the lack of significant enhancement of molecular nitric acid in solutions with $\leq$2 mol % H_2SO_4; fewer HSO_4^- ions in the interfacial region would have a much reduced impact on the number of water molecules able to participate in nitric acid dissociation. Support for this concentration dependent effect of sulfuric acid on nitric acid dissociation at the surface of ternary solutions is provided by bulk Raman studies.[37] These studies of $HNO_3-H_2SO_4-H_2O$ mixtures show that as the H_2SO_4 content increases/decreases, the HNO_3/NO_3^- ion equilibrium shifts such that the ν_3 band of the nitrate ion decreases/increases while the ν_1 band of molecular nitric acid increases/decreases in intensity.

6. Conclusions

Molecular HNO_3 has been directly observed in the top surface layers of binary HNO_3-H_2O and ternary $HNO_3-H_2SO_4-H_2O$ solutions using vibrational sum-frequency spectroscopy. Although this result is consistent with predictions from surface tension measurements and other surface spectroscopic studies,[20−22] the conclusions drawn from this work further advance understanding of the hydrogen-bonding character of these undissociated HNO_3 species and their adsorption at vapor/acid solution interfaces. The studies here present the first observation of two different hydrogen-bonded species of undissociated nitric acid at the acid solution surface of both binary and ternary mixtures. Frequencies of the NO_2 antisymmetric stretching mode in the region 1650−1700 cm^{-1} suggest that both of these species are hydrogen bonded to water. The frequencies of these species also suggest differences in the solvation environment of the acid NO_2 group in the interfacial region. A spectral feature at 1662 $\pm$ 2 cm^{-1} is attributed to a complex between HNO_3 and H_2O with hydrogen bonds to both the acid OH and NO_2 groups. By contrast, a second feature at 1690 $\pm$ 2 cm^{-1} is assigned to a monohydrate complex with a nonbonded NO_2 group. Such a weakly bonded molecular HNO_3 complex with water is unique to the sum-frequency experiment and is not observed in the interfacial region as defined by ATR-FTIR experiments. Given this, and because the NO_2 group of this monohydrate is free to protrude out into the vapor phase, a location in the topmost surface layer of the solution is proposed for this complex. The ternary $HNO_3-H_2SO_4-H_2O$ solution data here show that the adsorption of these two molecular HNO_3 species is enhanced at the surface compared to the binary HNO_3-H_2O solution, but that the enhancement depends on the concentration of sulfuric acid. For H_2SO_4 concentrations $\geq$10 mol %, the presence of undissociated nitric acid is significantly enhanced at the surface, whereas concentrations $\leq$2 mol % have little effect. This H_2SO_4 concentration dependent behavior is attributed to HSO_4^- (or H_2SO_4) species at the surface that bind water and interfere with the HNO_3 dissociation equilibrium and adsorption of molecular HNO_3 at the surface.

These results have implications for heterogeneous processes involving nitric and sulfuric acids at aqueous surfaces in the atmosphere, in which reaction kinetics and mechanisms could depend on the HNO_3 composition of the surface. For example, laboratory studies have shown that reactions between gaseous NO and molecular HNO_3 (and not NO_3^-) adsorbed in thin water films on silica surfaces produce reactive nitrogen species such as NO_2 and HONO that impact tropospheric pollution.[12] The presence of water on the solid surface was found to be critical.[14] This suggests that soils, dust particles, and solid surfaces in urban environments that adsorb nitric acid and water can provide sites for HNO_3 reactions with NO. The studies reported here demonstrate the potential role of such reactions involving molecular HNO_3 at liquid aerosol surfaces in the atmosphere.

The conclusions also have clear implications for gaseous uptake and hydrolysis reactions in the troposphere and stratosphere. For example, the hydrolysis of NO_2 at hydrated solid surfaces has been widely studied because it generates HONO, a major source of OH in the troposphere, as well as HNO_3.[10,11,51] A buildup of molecular HNO_3 bound to water at aqueous atmospheric surfaces could have an impact on NO_2 uptake and hydrolysis reaction rates. In the stratosphere, the hydrolysis of $ClONO_2$ and N_2O_5 on aqueous sulfuric acid droplets are important chlorine and NO_x processing reactions that also produce nitric acid.[52,53] Experiments have shown that the presence of nitric acid dissolved in sulfuric acid decreases both the $ClONO_2$ and N_2O_5 hydrolysis reaction probabilities.[53,54] Given the results of the present study, an enhancement in nitric acid−water complexes adsorbed at the surface of ternary $HNO_3/H_2SO_4/H_2O$ particles could interfere with the gaseous uptake of $ClONO_2$ and N_2O_5 and cause a reduction in the hydrolysis reaction rates. Because the microscopic composition of HNO_3 at aqueous aerosol surfaces can have a significant influence on gaseous uptake and reactivity, the insight provided here into the adsorption of molecular nitric acid at HNO_3/H_2O and $HNO_3/H_2SO_4/H_2O$ solution surfaces contributes to our understanding of heterogeneous processes in the atmosphere.

Acknowledgment. We thank the National Science Foundation (CHE-0243856) for support of this work.

References and Notes

(1) Knipping, E. M.; Lakin, M. J.; Foster, K. L.; et al. *Science* **2000**, *288*, 301.

(2) Liu, D.; Ma, G.; Levering, L. M.; Allen, H. C. *J. Phys. Chem. B* **2004**, *108*, 2252.

(3) Schnitzer, C.; Baldelli, S.; Shultz, M. J. *J. Phys. Chem. B* **2000**, *104*, 585.

(4) Jungwirth, P.; Tobias, D. *J. Phys. Chem. B* **2001**, *105*, 10468.

(5) Raymond, E. A.; Richmond, G. L. *J. Phys. Chem. B* **2004**, *108*, 5051.

(6) Ghosal, S.; Hemminger, J. C.; Bluhm, H.; et al. *Science* **2005**, *307*, 563.
(7) Petersen, P. B.; Saykally, R. J. *J. Phys. Chem. B* **2005**, *109*, 7976.
(8) Dang, L. X.; Chang, T.-M.; Roeselova, M.; Garrett, B. C.; Tobias, D. J. *J. Chem. Phys.* **2006**, *124*, 066101.
(9) Vrbka, L.; Mucha, M.; Minofar, B.; et al. *Curr. Opin. Colloid Interface Sci.* **2004**, *9*, 67.
(10) Finlayson-Pitts, B. J.; Wingen, L. M.; Sumner, A. L.; Syomin, D.; Ramazan, K. A. *Phys. Chem. Chem. Phys.* **2003**, *5*, 223.
(11) Ramazan, K. A.; Wingen, L. M.; Miller, Y.; et al. *J. Phys. Chem. A* **2006**, *110*, 6886.
(12) Rivera-Figueroa, A. M.; Sumner, A. L.; Finlayson-Pitts, B. J. *Environ. Sci. Technol.* **2003**, *37*, 548.
(13) Mochida, M.; Finlayson-Pitts, B. *J. Phys. Chem. A* **2000**, *104*, 9705.
(14) Saliba, N. A.; Yang, H.; Finlayson-Pitts, B. J. *J. Phys. Chem. A* **2001**, *105*, 10339.
(15) Zondlo, M. A.; Hudson, P. K.; Prenni, A. J.; Tolbert, M. A. *Ann. Rev. Phys. Chem.* **2000**, *51*, 473.
(16) Anthony, S. E.; Onasch, T. B.; Tisdale, R. T.; Disselkamp, R. S.; Tolbert, M. A. *J. Geophys. Res.* **1997**, *102*, 10777.
(17) Raymond, E. A.; Tarbuck, T. L.; Brown, M. G.; Richmond, G. L. *J. Phys. Chem. B* **2003**, *107*, 546.
(18) Morita, A.; Hynes, J. T. *Chem. Phys.* **2000**, *258*, 371.
(19) Morita, A.; Hynes, J. T. *J. Phys. Chem. B* **2002**, *106*, 673.
(20) Schnitzer, C.; Baldelli, S.; Campbell, D. J.; Shultz, M. J. *J. Phys. Chem. A* **1999**, *103*, 6383.
(21) Donaldson, D. J.; Anderson, D. *Geophys. Res. Lett.* **1999**, *26*, 3625.
(22) Yang, H.; Finlayson-Pitts, B. *J. Phys. Chem. A* **2001**, *105*, 1890.
(23) Shen, Y. R. *Nature* **1989**, *337*, 519.
(24) Eisenthal, K. B. *Chem. Rev.* **1996**, *96*, 1343.
(25) Richmond, G. L. *Chem. Rev.* **2002**, *102*, 2693.
(26) Kido Soule, M. C.; Hore, D. K.; Jaramillo-Fellin, D. M.; Richmond, G. L. *J. Phys. Chem. B* **2006**, *110*, 16575.
(27) Bain, C. D.; Davies, P. B.; Ong, T. H.; Ward, R. N. *Langmuir* **1991**, *7*, 1563.
(28) Goates, S. R.; Schofield, D. A.; Bain, C. D. *Langmuir* **1999**, *15*, 1400.
(29) Moore, F. G.; Becraft, K. A.; Richmond, G. L. *Appl. Spectrosc.* **2002**, *56*, 1575.
(30) Barnes, A. J.; Lasson, E.; Nielsen, C. J. *J. Mol. Struct.* **1994**, *322*, 165.
(31) Querry, M. R.; Taylor, I. L. *J. Chem. Phys.* **1980**, *74*, 2495.
(32) McGraw, G. E.; Bernitt, D. L.; Hisatsune, I. C. *J. Chem. Phys.* **1965**, *42*, 237.
(33) Salvador, P.; Curtis, J. E.; Tobias, D. J.; Jungwirth, P. *Phys. Chem. Chem. Phys.* **2003**, *5*, 3752.
(34) Minofar, B.; Vacha, R.; Wahab, A., et al. *J. Phys. Chem. B* **2006**, *110*, 15939.
(35) Waterland, M. R.; Kelly, A. M. *J. Chem. Phys.* **2000**, *113*, 6760.
(36) Davis, W.; Brun, H. J. d. *J. Inorg. Nucl. Chem.* **1964**, *26*, 1069.
(37) Minogue, N.; Riordan, E.; Dodeau, J. R. *J. Phys. Chem. A* **2003**, *107*, 4436.
(38) Hogfeldt, E. *Acta Chem. Scand.* **1963**, *17*, 785.
(39) Canagaratna, M.; Phillips, J. A.; Ott, M. E.; Leopold, K. R. *J. Phys. Chem. A* **1998**, *102*, 1489.
(40) Ritzhaupt, G.; Devlin, J. P. *J. Phys. Chem.* **1991**, *95*, 90.
(41) Tolbert, M. A.; Middlebrook, A. M. *J. Geophys. Res.* **1990**, *95*, 22423.
(42) Tao, F.-M.; Higgins, K.; Klemperer, W.; Nelson, D. D. *Geophys. Res. Lett.* **1996**, *23*, 1797.
(43) Bouteiller, Y. *Chem. Phys.* **2005**, *314*, 159.
(44) Rowland, B.; Fisher, M.; Devlin, J. P. *J. Chem. Phys.* **1991**, *95*, 1378.
(45) Devlin, J. P. *J. Chem. Phys.* **2000**, *112*, 5527.
(46) Martin, E.; George, C.; Mirabel, P. *Geophys. Res. Lett.* **2000**, *27*, 197.
(47) Myhre, C. E. L.; Grothe, H.; Gola, A. A.; Nielson, C. J. *J. Phys. Chem. A* **2005**, *109*, 7166.
(48) Mucha, M.; Frigato, T.; Levering, L. M.; et al. *J. Phys. Chem. B* **2005**, *109*, 7617.
(49) Baldelli, S.; Schnitzer, C.; Shultz, M. J.; Campbell, D. J. *J. Phys. Chem. B* **1997**, *101*, 10435.
(50) Shultz, M. J.; Baldelli, S.; Schnitzer, C.; Simonelli, D. *J. Phys. Chem. B* **2002**, *106*, 5313.
(51) Goodman, A. L.; Underwood, G. M.; Grassian, V. H. *J. Phys. Chem. A* **1999**, *103*, 7217.
(52) Zhang, R.; Leu, M.-T.; Keyser, L. F. *J. Phys. Chem.* **1994**, *98*, 13563.
(53) Hanson, D. R. *J. Phys. Chem. A* **1998**, *102*, 4794.
(54) Zhang, R.; Leu, M.-T.; Keyser, L. F. *Geophys. Res. Lett.* **1995**, *22*, 1493.